Research Paper

Regional biomechanical imaging of liver cancer cells

Weiwei Pei[1*], Jiayao Chen[2*], Chao Wang[4], Suhao Qiu[5], Jianfeng Zeng[2], Mingyuan Gao[2], Bin Zhou[3], Dan Li[3], Michael S. Sacks[6], Lin Han[4], Hong Shan[3✉], Wentao Hu[1✉], Yuan Feng[5✉], Guangming Zhou[1✉]

1. State Key Laboratory of Radiation Medicine and Protection, School of Radiation Medicine and Protection, Collaborative Innovation Center of Radiological Medicine of Jiangsu Higher Education Institutions, Soochow University, Suzhou 215123, China
2. Center for Molecular Imaging and Nuclear Medicine, School of Radiological and Interdisciplinary Sciences (RAD-X), Soochow University, Collaborative Innovation Center of Radiation Medicine of Jiangsu Higher Education Institutions, Suzhou 215123, China
3. Guangdong Provincial Engineering Research Center of Molecular Imaging, the Fifth Affiliated Hospital, Sun Yat-sen University, Zhuhai 519000, China
4. School of Biomedical Engineering, Science and Health Systems, Drexel University, Philadelphia, PA 19104, USA
5. Institute for Medical Imaging Technology, School of Biomedical Engineering, Shanghai Jiao Tong University, Shanghai 200240, China
6. Willerson Center for Cardiovascular Modeling and Simulation, Institute for Computational Engineering & Sciences, the University of Texas at Austin, TX 78712, USA

*The two authors contributed equally.

✉ Corresponding authors: Yuan Feng, Ph.D. Shanghai Jiao Tong University, School of Biomedical Engineering, Institute for Medical Imaging Technology, Shanghai 200240, China; Wentao Hu, Ph.D. Soochow University, School of Radiation Medicine and Protection, State Key Laboratory of Radiation Medicine and Protection, Suzhou 215123, China; Hong Shan, Ph.D. Guangdong Provincial Engineering Research Center of Molecular Imaging, the Fifth Affiliated Hospital, Sun Yat-sen University, Zhuhai 519000, China; Guangming Zhou, Ph.D. Soochow University, School of Radiation Medicine and Protection, State Key Laboratory of Radiation Medicine and Protection, Suzhou 215123, China.

Email: gmzhou@suda.edu.cn

Abstract

Liver cancer is one of the leading cancers, especially in developing countries. Understanding the biomechanical properties of the liver cancer cells can not only help to elucidate the mechanisms behind the cancer progression, but also provide important information for diagnosis and treatment. At the cellular level, we used well-established atomic force microscopy (AFM) techniques to characterize the heterogeneity of mechanical properties of two different types of human liver cancer cells and a normal liver cell line. Stiffness maps with a resolution of 128x128 were acquired for each cell. The distributions of the indentation moduli of the cells showed significant differences between cancerous cells and healthy controls. Significantly, the variability was even greater amongst different types of cancerous cells. Fitting of the histogram of the effective moduli using a normal distribution function showed the Bel7402 cells were stiffer than the normal cells while HepG2 cells were softer. Morphological analysis of the cell structures also showed a higher cytoskeleton content among the cancerous cells. Results provided a foundation for applying knowledge of cell stiffness heterogeneity to search for tissue-level, early-stage indicators of liver cancer.

Key words: biomechanics; AFM; indentation; liver cancer; cell stiffness

Introduction

Liver cancer is one of the most fast growing cancer forms in terms of new incidents and death cases [1]. It is known that cells can sense mechanical forces and deformations and transduce into biological response [2] [3] [4] [5] [6]. Biomechanical properties of cancer cells have shown to be closely related with cancer pathology and metastasis state abnormalities [7] [8]. It is also found that the biomechanical changes were correlated with the cell-cell communications [9]

and microenvironment [10] [11]. Understanding the biomechanical properties of tumor cells can not only help to elucidate the mechanisms behind disease progression, but also provide important information for cancer diagnosis and treatment [12] [13] [14].

Many methods have been used to measure the mechanical properties of individual cells, such as atomic force microscopy (AFM), micropipette aspiration, optical tweezers, etc. [15] [16] [17]. Among

these methods, AFM-based nanoindentation is one of the most widely used modality to measure the cellular structures [18] [19] and probe the mechanical properties of living cells [20] [21] [22]. It has been used to measure micro-scale structures of cells [23] [24] [25] [21] and microorganisms [22], as well as macro-scale structures such as cartilage tissue [26] [27] and brain tissue [28]. In this study, we used AFM to characterize the mechanical properties of liver cancer cells. Although many studies have investigated the mechanical properties of tumor cells [15] [21] [24], few studies have investigated the mechanical properties of liver cancer cells. Wu et al. was among the first to investigate the viscoelastic properties of hepatocytes and hepatocellular carcinoma (HCC) cells using micropipette techniques [29]. Using AFM nanoindentation, Grady [30] also investigated the elastic properties of the HUH-7 (HCC) cells.

At the tissue level, studies characterizing the mechanical properties of soft tissues have highlighted the heterogeneity of many tissues [31] [32]. For example, Plodinec [33] used AFM to characterize the distribution of the mechanical properties at the tissue level as a biomarker for breast cancer diagnosis. At the cellular level, cells have complex surface structures containing a variety of components such as lipid and protein. In addition, beneath the plasma membrane, cytoskeleton of the cell is also a heterogeneous meshwork. Therefore, the mechanical properties of cells are essentially heterogeneous. Guo [34] studied the distributions of elastic parameters to characterize the cell properties. Hecht [35] mapped out the viscoelastic properties of cells with a resolution of 50 × 50 and a pixel resolution of 640–950 nm. For higher resolution mapping of effective modulus, Smolyakov [36] imaged elastic module of bacteria samples with a resolution up to 128×128 for a region of interest about $1.5× 1.5 \ \mu m^2$. Although differences in mechanical properties between healthy and cancerous tissue have long been studied as biomarkers of various cancers, a feature that has not yet been exploited is mechanical heterogeneity.

In this study, we used AFM nanoindentation method to investigate the biomechanical properties of both liver cancer cells and normal liver cells. Mechanical heterogeneity properties were mapped

out with a fine resolution. Distribution features of the effective modulus were compared between the cancerous and normal cells. Results provided biomechanical properties for potential application in liver cancer diagnosis and prognosis.

Materials and methods

Cell preparation

Hepatoma cells including Bel7402, HepG2 and human normal liver cell line L02 were purchased from Shanghai Cell Bank of Chinese Academy of Sciences. Cells were cultured in RPMI-1640 medium (Gibco, Grand Island, NY, USA) supplemented with 10% fetal bovine serum (FBS, Gibco, Grand Island, NY, USA), 1% penicillin sodium and 100 μg/mL streptomycin, at 37°C in 5% CO2 in a humidified incubator (Thermo Scientific, Asheville, NC, USA). Normal and hepatoma cell cultures were both maintained in FBS medium under the same conditions. The cells were cultured until tightly adhered to the micropatterned glass-bottom culture dishes. Cells were grown to 10%-20% of their confluency before tests. The 60-mm cell culture dishes were mounted on the sample stage of the AFM. All scanning and measurements were performed on proliferating viable cells maintained to room temperature in Phosphate Buffer Saline (PBS) within 1–2 hours after removal of growth medium and rinse for three times by PBS.

AFM-nanoindentation

Indentation tests were performed using a combined atomic microscope with an inverted optical microscope (BioScope Resolve Atomic Force Microscope) at room temperature. Probes with a nominal spring constant of 0.10 N/m are chosen for the experiment (MLCT type E tip, Bruker Co. Ltd., Billerica, MA, USA). We used the Peak Force Quantitative Nanomechanical Mapping in fluid to measure the indentation responses at each testing point. The measurements were carried out with cells submerged within PBS in a liquid testing mode (Figure 1). A field of view (FOV) of 50×50 μm² was selected for mapping the elastic modulus of the cell with an image resolution of 128x128.
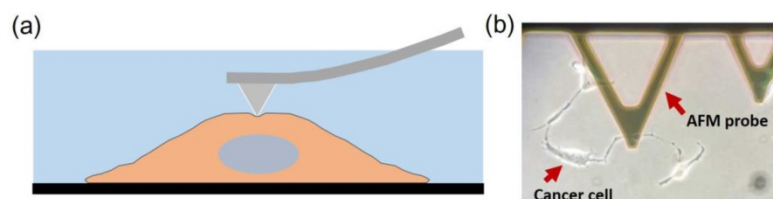

Figure 1. (a) Illustration of nanoindentation of cancer cells using AFM. The measurements were carried out with live cells submerged within PBS solution. **(b)** A microscope image showing a typical measurement of liver cancer cell with a MLCT E-type probe.

Hertz and Sneddon models were the most used method for characterizing cell properties [25] [37]. In this study, the indentation depth is more than 10 times larger than that of the tip radius, therefore the Sneddon model was adopted [34]. The four sided pyramid AFM problem was usually modeled by pyramid [38], and the effective modulus could be estimated by

$$E = \frac{\pi}{2} \frac{(1-v^2)}{tan(\alpha)} \frac{F}{\delta^2} \qquad (1)$$

where F is the indentation force, δ is the corresponding indentation displacement, α is the semi-included angle of the pyramid tip, and v is the Poisson's ratio. We used $v = 0.5$ since the cells could be treated as incompressible [14] [34] [38]. The modulus map was estimated for each of the 16,384 indentation points using the force-displacement curve acquired. To reduce the substrate effect due to the model assumption of a semi-infinite space, we selected the top region (above the half of the cell height) of the cell covering the nucleus and major cell contents for analysis. This selection guarantees that the thickness of the sample is more than 50 times of the tip radius.

Based on the modulus images, histogram of the probability distribution function was fitted with a normal distribution. The mean value μ and the standard deviation σ of the distribution with their 95% confidence intervals were estimated for each cell. The average values of μ and σ were also compared with respect to the regions acquired from the 6 Bel7402 cells, 6 HepG2 cells, and 6 normal liver cells. To see the differences of effective modulus between each cell type, the measured indentation points for each cell were grouped together for student's t-tests at a significance level of 5%.

Confocal microscopy

To observe the microstructure of each cell, samples in the glass-bottom dishes were fixed with freshly prepared 4% formaldehyde (Sinopharm Chemical Reagent Co. Ltd.) in PBS for 10 min at room temperature. After fixation, we washed samples with PBS for three times and added 0.1% Triton X-100 (Sigma Aldrich Co. Ltd., Shanghai) in PBS with 1% bovine serum albumin (MesGen, Shanghai Hongsheng biotechnology Co. Ltd) to each for 5 min. After this permeabilization, fluorescein–phalloidin solution (MesGen MF8203, Shanghai Hongsheng Biotechnology Co. Ltd) was applied for 20 min at room temperature inside a covered container during the incubation. The samples were subsequently washed with PBS for three times. We followed the protocol recommended in the product Hoechst 33342 (Sigma Aldrich Co. Ltd, Shanghai) for the cell nucleus

staining. Confocal images were taken using a laser scanning confocal microscope (Olympus FV1200, Japan).

Table 1. Estimated normal distribution parameters for each cell and the corresponding 95% confidence intervals for the parameters. μ and σ are the mean and standard deviation values for the normal distribution.

	μ (kPa)	σ (kPa)	Average μ (kPa)
Bel7402	0.256±0.003	0.053±0.002	0.154
	0.105±0.001	0.039±8.40x10-4	
	0.162±0.003	0.05± 0.002	
	0.130±8.60x10-4	0.025±6.09x10-4	
	0.131±0.001	0.033±9.80x10-4	
	0.139±0.004	0.731±0.002	
HepG2	0.030±9.22x10-4	0.021±6.52x10-4	0.063
	0.041±7.83x10-4	0.014±5.54x10-4	
	0.058±9.31x10-4	0.049±6.59x10-4	
	0.092±0.001	0.023±8.26x10-4	
	0.094±8.13x10-4	0.021±5.75x10-4	
	0.060±9.31x10-4	0.020±6.59x10-4	
L02	0.165±0.002	0.050±0.002	0.174
	0.379±0.005	0.079±0.003	
	0.144±0.003	0.043±0.002	
	0.181±0.002	0.042±0.002	
	0.067±0.004	0.067±0.003	
	0.109±0.006	0.089±0.004	

Results

Typical height images of the 3 types of cells showed that cancerous cells were about 2-3 times larger than the normal liver cells (Figure 2). In addition, we also observed the morphological differences between the cell shapes where the cancerous cells have branches of tentacles stretching out of the cell bodies. Typical force-displacement curves of the nanoindentation from different cells showed different effective modulus, where from stiff to soft were Bel7402, L02, and HepG2 cells.

The effective moduli were mapped out with respect to approximately upper 50% height of each cell (Figure 3). We observed that Bel7402 and HepG2 cells had higher moduli than that of L02 cells. Analysis of the probability density function (PDF) of the effective modulus distribution showed significant differences between each cell (Figure 3). For cancerous cells, the mean effective moduli of the Bel7402 were significantly higher than that of HepG2. The L02 cells appeared to have a large standard deviation of effective modulus with a relatively higher value than HepG2 cells. The estimated effective modulus distribution parameters for each cell were summarized in Table 1.The maximum and minimum mean elastic moduli were 0.256 and 0.030 for Bel7402 and HepG2 cells, respectively. The maximum and minimum standard deviation values of the elastic moduli were also observed for Bel7402 and HepG2 cells, which are 0.731 and 0.014, respectively. Ranking

from maximum to minimum values of the overall average modulus, we observed an order of Bel7402, L02, and HepG2. One-way ANOVA analysis showed that the mean elastic moduli were significantly different between the three cells but no significant differences were observed for the standard deviation values.

Confocal images of the cells showed that the Bel7402 cells have relatively larger cytoskeleton structures. We analyzed the cytoskeleton ratio of the cells with respect to the whole cell in terms of the areas (Figure 4). The mean ratios were 0.42±0.11, 0.39±0.11, and 0.07±0.03 for Bel7402, HepG2, and L02 cells, respectively. The only significant differences were found between the normal cells and the cancerous cells (student t-test, $p<0.05$).
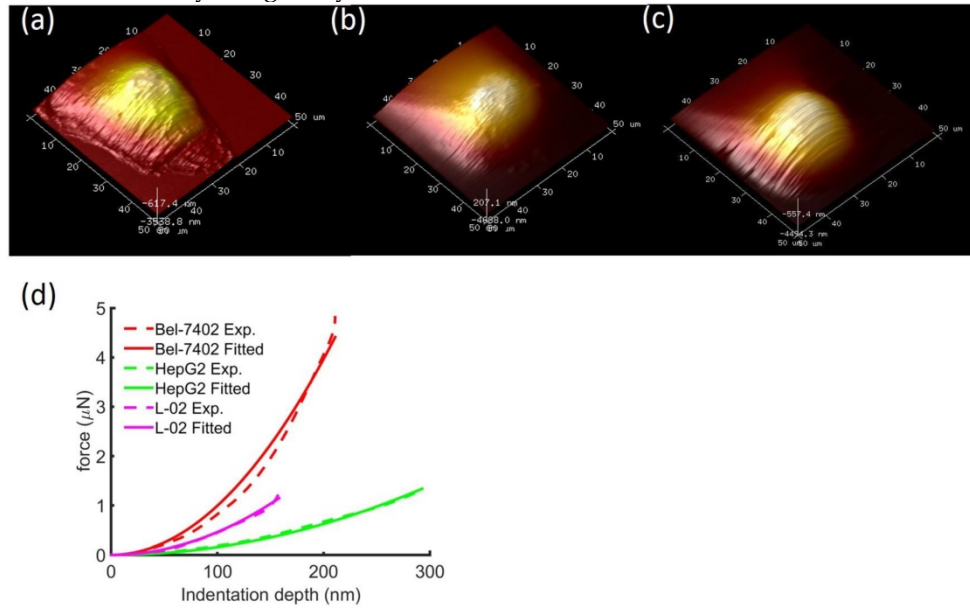

Figure 2. Typical height images of **(a)** Bel7402, **(b)** HepG2, and (c) L02. The image FOV was 50×50μm². Comparison of typical indentation force-displacement curves between the three different cell types **(d)**. The experiment curves were fitted with Sneddon model of Eq. (1). The distinguishable curves of the three cells showed stiffness differences between the cells.
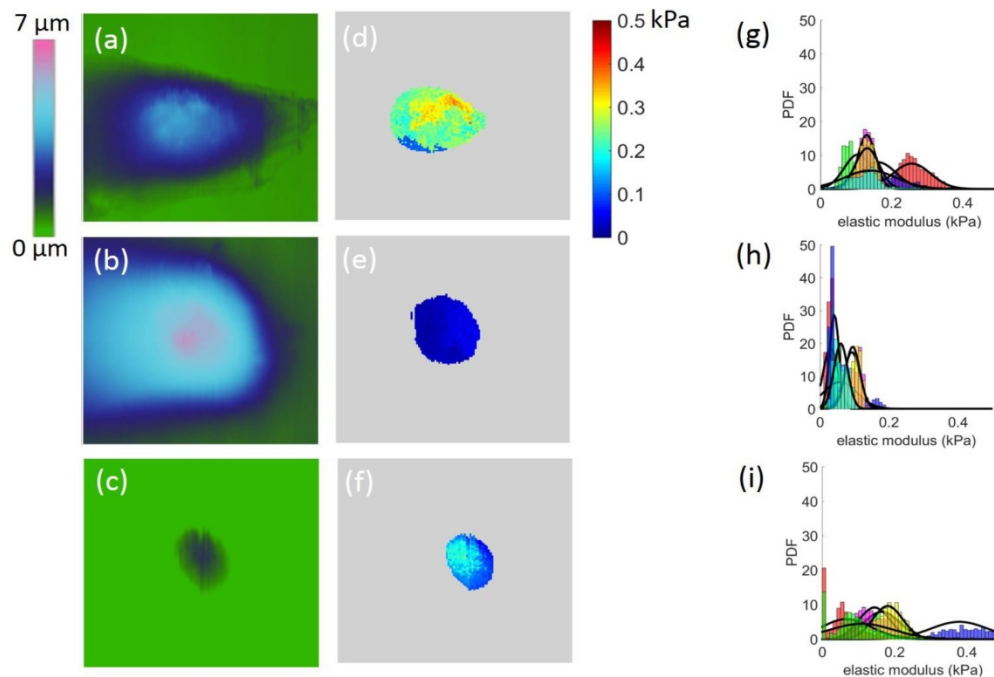

Figure 3. Height images **(a-c)** and the corresponding modulus map **(d-f)** for Bel7402, HepG2, and L02 cells, respectively. The corresponding elastic moduli above the half height of the cells were selected for analysis. The field of view for each image is 50×50μm². The estimated probability distribution function (PDF) of the effective modulus distribution for (g) Bel7402, (h) HepG2, and (i) L02 cells. A normal distribution function was fitted to each histogram.
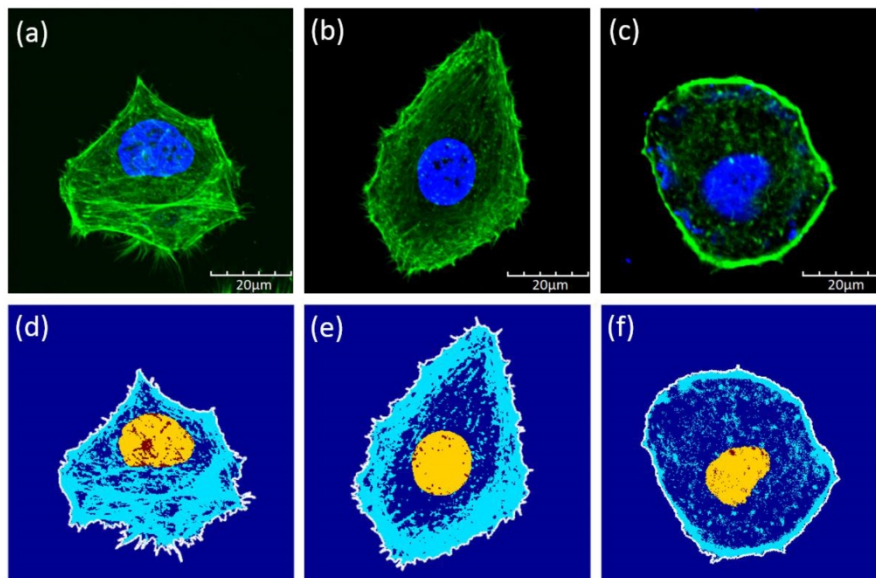
Figure 4. Confocal images of **(a)** Bel7402, **(b)** HepG2, and **(c)** L02 cells. Although the sizes of the cells were similar between each type, the cytoskeleton structures were different among these cells. Illustrations of the cell boundaries (white line), nucleus (yellow region), and the cytoskeleton (blue lines) for **(d)** Bel7402, **(e)** HepG2, and **(f)** L02 cells. The structures were extracted based on the confocal images of Figure 4.

Discussion

In this study, we investigated the effective modulus and its heterogeneity of liver cancer cells. Using AFM nanoindentation techniques, we observed that, the cancerous cells and the normal cells had significant different distribution of the effective modulus in the cellular level. Significant differences of the mean modulus were also found between the three types of cells. Analysis of the cellular structure shed lights on the mechanical behaviors.

Experimental measurement

Many studies have used AFM nanoindentation to investigate the effective modulus of cancerous cells. Some studies have shown that cervical cancer cells (HeLa) have a softer hardness than normal human uterine epithelial cells. Similarly, malignant (MCF-7) breast cells were found to have an apparent Young's modulus significantly lower (1.4-1.8 times) than that of their non-malignant (MCF-10A) counterparts, but limited data were available for liver cancer cells [39] [21]. Our study shows that there is no significant difference in the hardness between normal liver cells line and liver tumor cell lines, this may be dependent on different cell lines. In addition, most of investigations focused on the overall mechanical response of the cancerous cells, using a spherical bead indenter or pyramid indenter with respect to selected points on the cell [40]. In this study, we provided a detailed mapping of the effective modulus of two different types of liver cancer cells. Unlike cells such as pancreatic beta cells that demonstrated strong adhesion effects during indentation, we did not notice

significant adhesion effects for all the cancerous and normal liver cells [41]. We found that the effective modulus of the liver cancer cells ranged from 0.03-0.26 kPa, similar to that of the cancerous breast epithelial cells [24]. Grady [30] found the median Young's modulus of the HUH-7 cells was 0.3 kPa, which is similar to the effective modulus of Bel7402 cells we measured.

Influences of morphological structure

It has been known that the cellular structure such as cytoskeleton contributed to the mechanical properties of cells [42]. Using gastrointestinal tumor and malaria cells, Suresh [7] found that the effective modulus of cells increased or decreased due to membrane or cytoskeleton reorganization. It was also found that mechanical properties of the cells also depend on the level of cancer transformation. With a low level of transformation, cells were softer than that with a higher level of transformation [43]. In this study, we observed that different types of liver cancer cells had significant different effective moduli and the heterogeneous properties. However, by comparing the estimated structure ratio of the cytoskeleton, we found no significant differences between the cancer cells. This indicates that the morphological structure of the cells may not be the main contributor to the mechanical properties of the cells, rather the properties of the structure such as the cytoskeleton or membrane could play a major role.

Sun [44] and Wu [45] founded that differences in cell cytoskeleton (F-actin) were accompanied with changes in the cell migration ability and Young's modulus. Studies have shown that disruption of

microtubule dynamics could affect cancer cell effectively [5] [30]. Both Grady [30] and Wu [29] found that upon removal of cytoskeleton structures, the elastic properties of the HCC cells decreased. Although we did not notice a significant difference in the volume ratio of cytoskeletons between the cancerous cells, a significant lower composition of cytoskeleton was observed for the normal liver cells. Besides, it has been found that Bel7402 cells have higher migration and invasive capacity than HepG2 cells [46]. We postulate that a higher volume ratio of the cytoskeleton structure could contribute to higher migration ability among the tested cancerous cells.

Correlation between the tissue and cellular level

Using AFM, the measured effective modulus can be used to distinguish normal and cancerous breast cancer cells [24] [47]. For most cancerous cells, the effective modulus was lower than the corresponding normal cells [21]. Li [24] are among the first to investigate the mechanical properties of breast cancer cells and observed significantly lower apparent Young's modulus of the Malignant (MCF-7) breast cells than that of the non-malignant (MCF-10A) counterparts. We observed that HepG2 was softer than the normal liver cells. However, no significant differences were observed between the Bel7402 and normal liver cells. These type-dependent properties were similar to that of the cervix cancer cells, where CRL2614 cells were stiffer [48] and primary cancer cells were softer [49]. Therefore, we showed that cancerous cells were not necessarily softer than normal cells, the hardness of the cells depend on the specific categories and phenotypes.

In vivo characterization of the mechanical properties of liver cancer tissue showed that the cancerous tissues were stiffer than that of the normal tissues [50] [51]. Similar stiffening behavior in the tissue level was also observed for other cancers such as breast cancer [52]. The stiffer behavior at the tissue level were different from that at the cellular level, where we found that only Bel7402 cells were stiffer than the normal liver cells. The differences of the mechanical properties in the cellular and tissue level revealed that besides the mechanical properties of the cells, structures such as extra cellular matrix (ECM) play an important role in the tissue level behavior. In fact, studies have already pointed out that rigid tumors were stiffer than normal tissues because of a stiffer ECM [53]. However, cancerous cells that were either stiffer or softer than the normal cells indicated a variation of the roles of ECM in affecting the tissue level mechanics. This provided new clues in understanding the mechanotransduction of cancer cells [53] [54] [55] [56].

Limitations and future studies

In this study, we only mapped out the effective properties of live cancer cells. However, elastic properties cannot represent the full mechanical characteristics of cancer cells, since viscoelastic behaviors have been observed for many different types of cells [57]. Future studies involve finding a way to map out the viscoelastic properties of a live cell within a reasonable time frame. In addition, we will investigate the structural and mechanical properties of the ECM of liver cancer tissues.

Conclusions

In this study, we used AFM nanoindentation to characterize the mechanical properties of cancerous and normal liver cells. Elastic modulus with a refined resolution were acquired and analyzed. Distinct effective modulus and its distributions were found for each cell type, while significant differences of the effective moduli were found between cell types. The Bel7402 cells had the highest magnitude of effective modulus while HepG2 had the lowest modulus. Although the dispersion of the elastic module was different for each cell, no significant difference was found. Analysis of the morphological structure showed a significantly lower volume ratio of the normal liver cells than the cancerous cells. The results provided helpful hints for understanding the cellular behavior of liver cancer cells as well as the indications for understanding the mechanical differences between cellular and tissue levels.

Acknowledgement

Competing Interests

The authors have declared that no competing interest exists.

References

1. Siegel RL, Miller KD, Jemal A. Cancer statistics, 2016. CA Cancer J Clin. 2016; 66: 7-30.
2. Ji BH, Bao G. Cell and Molecular Biomechanics: Perspectives and Challenges. Acta Mech Solida Sin. 2011; 24: 27-51.

3. Shakiba D, Babaei B, Saadat F, Thomopoulos S, Genin GM. The fibrous cellular microenvironment, and how cells make sense of a tangled web. P Natl Acad Sci USA. 2017; 114: 5772-4.

4. Mierke CT. The fundamental role of mechanical properties in the progression of cancer disease and inflammation. Rep Prog Phys. 2014; 77.

5. Moeendarbary E, Harris AR. Cell mechanics: principles, practices, and prospects. Wires Syst Biol Med. 2014; 6: 371-88.

6. Long MJ, Pan Y, Lin HC, Hedstrom L, Xu B. Cell compatible trimethoprim-decorated iron oxide nanoparticles bind dihydrofolate reductase for magnetically modulating focal adhesion of mammalian cells. J Am Chem Soc. 2011; 133: 10006-9.

7. Suresh S, Spatz J, Mills JP, Micoulet A, Dao M, Lim CT, et al. Connections between single-cell biomechanics and human disease states: gastrointestinal cancer and malaria. Acta Biomaterialia. 2005; 1: 15-30.

8. Suresh S. Biomechanics and biophysics of cancer cells. Acta Biomaterialia. 2007; 3: 413-38.

9. Guz NV, Patel SJ, Dokukin ME, Clarkson B, Sokolov I. AFM study shows prominent physical changes in elasticity and pericellular layer in human acute leukemic cells due to inadequate cell-cell communication. Nanotechnology. 2016; 27.

10. Genin GM, Shenoy VB, Peng GCY, Buehler MJ. Integrated Multiscale Biomaterials Experiment and Modeling. Acs Biomater Sci Eng. 2017; 3: 2628-32.

11. Guo XY, Bonin K, Scarpinato K, Guthold M. The effect of neighboring cells on the stiffness of cancerous and non-cancerous human mammary epithelial cells. New J Phys. 2014; 16.

12. Lee GYH, Lim CT. Biomechanics approaches to studying human diseases. Trends Biotechnol. 2007; 25: 111-8.

13. Discher D, Dong C, Fredberg JJ, Guilak F, Ingber D, Janmey P, et al. Biomechanics: Cell Research and Applications for the Next Decade. Ann Biomed Eng. 2009; 37: 847-59.

14. Babaei B, Davarian A, Lee SL, Pryse KM, McConnaughey WB, Elson EL, et al. Remodeling by fibroblasts alters the rate-dependent mechanical properties of collagen. Acta Biomaterialia. 2016; 37: 28-37.

15. Calzado-Martin A, Encinar M, Tamayo J, Calleja M, Paulo AS. Effect of Actin Organization on the Stiffness of Living Breast Cancer Cells Revealed by Peak-Force Modulation Atomic Force Microscopy. Acs Nano. 2016; 10: 3365-74.

16. Han B, Nia HT, Wang C, Chandrasekaran P, Li Q, Chery DR, et al. AFM-Nanomechanical Test: An Interdisciplinary Tool That Links the Understanding of Cartilage and Meniscus Biomechanics, Osteoarthritis Degeneration, and Tissue Engineering. Acs Biomater Sci Eng. 2017; 3: 2033-49.

17. Pan Y, Long MJC, Lin HC, Hedstrom L, Xu B. Magnetic nanoparticles for direct protein sorting inside live cells. Chem Sci. 2012; 3: 3495-9.

18. Weafer PP, Reynolds NH, Jarvis SP, McGarry JP. Single cell active force generation under dynamic loading - Part I: AFM experiments. Acta Biomaterialia. 2015; 27: 236-50.

19. Reynolds NH, McGarry JP. Single cell active force generation under dynamic loading - Part II: Active modelling insights. Acta Biomaterialia. 2015; 27: 251-63.

20. Dufrene YF, Ando T, Garcia R, Alsteens D, Martinez-Martin D, Engel A, et al. Imaging modes of atomic force microscopy for application in molecular and cell biology. Nat Nanotechnol. 2017; 12: 295-307.

21. Lekka M. Discrimination Between Normal and Cancerous Cells Using AFM. Bionanoscience. 2016; 6: 65-80.

22. Zeng WJ, Yang H, Xuan GH, Dai LT, Hu YX, Hu SJ, et al. Longitudinal Study of the Effects of Environmental pH on the Mechanical Properties of Aspergillus niger. Acs Biomater Sci Eng. 2017; 3: 2974-9.

23. Guz N, Dokukin M, Kalaparthi V, Sokolov I. If Cell Mechanics Can Be Described by Elastic Modulus: Study of Different Models and Probes Used in Indentation Experiments. Biophys J. 2014; 107: 564-75.

24. Li QS, Lee GYH, Ong CN, Lim CT. AFM indentation study of breast cancer cells. Biochem Bioph Res Co. 2008; 374: 609-13.

25. Li Q, Qu FN, Han B, Wang C, Li H, Mauck RL, et al. Micromechanical anisotropy and heterogeneity of the meniscus extracellular matrix. Acta Biomaterialia. 2017; 54: 356-66.

26. McLeod MA, Wilusz RE, Guilak F. Depth-dependent anisotropy of the micromechanical properties of the extracellular and pericellular matrices of articular cartilage evaluated via atomic force microscopy. Journal of Biomechanics. 2013; 46: 586-92.

27. Park S, Costa KD, Ateshian GA. Microscale frictional response of bovine articular cartilage from atomic force microscopy. Journal of Biomechanics. 2004; 37: 1679-87.

28. Elkin BS, Ilankovan AI, Morrison B. A Detailed Viscoelastic Characterization of the P17 and Adult Rat Brain. J Neurotraum. 2011; 28: 2235-44.

29. Wu ZZ, Zhang G, Long M, Wang HB, Song GB, Cai SX. Comparison of the viscoelastic properties of normal hepatocytes and hepatocellular carcinoma cells under cytoskeletal perturbation. Biorheology. 2000; 37: 279-90.

30. Grady ME, Composto RJ, Eckmann DM. Cell elasticity with altered cytoskeletal architectures across multiple cell types. J Mech Behav Biomed Mater. 2016; 61: 197-207.

31. Prange MT, Margulies SS. Regional, directional, and age-dependent properties of the brain undergoing large deformation. J Biomech Eng. 2002; 124: 244-52.

32. Feng Y, Okamoto RJ, Namani R, Genin GM, Bayly PV. Measurements of mechanical anisotropy in brain tissue and implications for transversely isotropic material models of white matter. J Mech Behav Biomed Mater. 2013; 23: 117-32.

33. Plodinec M, Loparic M, Monnier CA, Obermann EC, Zanetti-Dallenbach R, Oertle P, et al. The nanomechanical signature of breast cancer. Nat Nanotechnol. 2012; 7: 757-65.

34. Guo Q, Xia Y, Sandig M, Yang J. Characterization of cell elasticity correlated with cell morphology by atomic force microscope. J Biomech. 2012; 45: 304-9.

35. Hecht FM, Rheinlaender J, Schierbaum N, Goldmann WH, Fabry B, Schaffer TE. Imaging viscoelastic properties of live cells by AFM: power-law rheology on the nanoscale. Soft Matter. 2015; 11: 4584-91.

36. Smolyakov G, Formosa-Dague C, Severac C, Duval RE, Dague E. High speed indentation measures by FV, QI and QNM introduce a new understanding of bionanomechanical experiments. Micron. 2016; 85: 8-14.

37. Cappella B, Kaliappan SK, Sturm H. Using AFM force-distance curves to study the glass-to-rubber transition of amorphous polymers and their elastic-plastic properties as a function of temperature. Macromolecules. 2005; 38: 1874-81.

38. Lekka M, Gil D, Pogoda K, Dulinska-Litewka J, Jach R, Gostek J, et al. Cancer cell detection in tissue sections using AFM. Arch Biochem Biophys. 2012; 518: 151-6.

39. Hayashi K, Iwata M. Stiffness of cancer cells measured with an AFM indentation method. J Mech Behav Biomed. 2015; 49: 105-11.

40. Lim CT, Zhou EH, Quek ST. Mechanical models for living cells - A review. Journal of Biomechanics. 2006; 39: 195-216.

41. Zhu XY, Siamantouras E, Liu KK, Liu X. Determination of work of adhesion of biological cell under AFM bead indentation. J Mech Behav Biomed. 2016; 56: 77-86.

42. Wang YX, Botvinick EL, Zhao YH, Berns MW, Usami S, Tsien RY, et al. Visualizing the mechanical activation of Src. Nature. 2005; 434: 1040-5.

43. Efremov YM, Lomakina ME, Bagrov DV, Makhnovskiy PI, Alexandrova AY, Kirpichnikov MP, et al. Mechanical properties of fibroblasts depend on level of cancer transformation. Bba-Mol Cell Res. 2014; 1843: 1013-9.

44. Sun JH, Luo Q, Liu LL, Zhang BY, Shi YS, Ju Y, et al. Biomechanical profile of cancer stem-like cells derived from MHCC97H cell lines. Journal of Biomechanics. 2016; 49: 45-52.

45. Wu LJ, Wang XB, Liu QH, Leung AW, Wang P, Xu CS. Sinoporphyrin sodium mediated photodynamic therapy inhibits the migration associated with collapse of F-actin filaments cytoskeleton in MDA-MB-231 cells. Photodiagn Photodyn. 2016; 13: 58-65.

46. Chen L, Li M, Li Q, Wang CJ, Xie SQ. DKK1 promotes hepatocellular carcinoma cell migration and invasion through beta-catenin/MMP7 signaling pathway. Mol Cancer. 2013; 12: 157.

47. Corbin EA, Kong F, Lim CT, King WP, Bashir R. Biophysical properties of human breast cancer cells measured using silicon MEMS resonators and atomic force microscopy. Lab Chip. 2015; 15: 839-47.

48. Zhao XQ, Zhong YX, Ye T, Wang DJ, Mao BW. Discrimination Between Cervical Cancer Cells and Normal Cervical Cells Based on Longitudinal Elasticity Using Atomic Force Microscopy. Nanoscale Res Lett. 2015; 10: 1-8.

49. Iyer S, Gaikwad RM, Subba-Rao V, Woodworth CD, Sokolov I. Atomic force microscopy detects differences in the surface brush of normal and cancerous cells. Nat Nanotechnol. 2009; 4: 389-93.

50. Hennedige TP, Hallinan JTPD, Leung FP, Teo LLS, Iyer S, Wang G, et al. Comparison of magnetic resonance elastography and diffusion-weighted imaging for differentiating benign and malignant liver lesions. Eur Radiol. 2016; 26: 398-406.

51. Venkatesh SK, Yin M, Glockner JF, Takahashi N, Araoz PA, Talwalkar JA, et al. MR elastography of liver tumors: Preliminary results. Am J Roentgenol. 2008; 190: 1534-40.

52. Ramiao NG, Martins PS, Rynkevic R, Fernandes AA, Barroso M, Santos DC. Biomechanical properties of breast tissue, a state-of-the-art review. Biomech Model Mechan. 2016; 15: 1307-23.

53. Huang S, Ingber DE. Cell tension, matrix mechanics, and cancer development. Cancer Cell. 2005; 8: 175-6.

54. Humphrey JD, Dufresne ER, Schwartz MA. Mechanotransduction and extracellular matrix homeostasis. Nat Rev Mol Cell Bio. 2014; 15: 802-12.

55. Iskratsch T, Wolfenson H, Sheetz MP. Appreciating force and shape - the rise of mechanotransduction in cell biology. Nat Rev Mol Cell Bio. 2014; 15: 825-33.

56. Mouw JK, Ou GQ, Weaver VM. Extracellular matrix assembly: a multiscale deconstruction. Nat Rev Mol Cell Bio. 2014; 15: 771-85.

57. Rother J, Noding H, Mey I, Janshoff A. Atomic force microscopy-based microrheology reveals significant differences in the viscoelastic response between malign and benign cell lines. Open Biol. 2014; 4.